PHYSICAL REVIEW E

STATISTICAL PHYSICS, PLASMAS, FLUIDS, AND RELATED INTERDISCIPLINARY TOPICS

THIRD SERIES, VOLUME 61, NUMBER 4 PART B **APRIL 2000**

ARTICLES

Geometry and dynamics of invasion percolation with correlated buoyancy

Jean Schmittbuhl and Alex Hansen*
Département Terre Atmosphère Océan, Ecole Normale Supérieure, 24 rue Lhomond, F-75231 Paris Cedex 05, France

Harold Auradou
Groupe Matière Condensée et Matériaux, Université de Rennes 1, F-320042 Rennes Cedex, France

Knut Jørgen Måløy
Fysisk Institutt, Universitetet i Oslo, Postboks 1048 Blindern, N-0316 Oslo, Norway

(Received 25 May 1999)

We study an invasion percolation model for drainage where the disorder comes partly from capillary thresholds and partly from height differences in a rough self-affine landscape. As a function of the buoyancy, the geometry of the invaded clusters changes dramatically. Long-range correlations from the fracture topography induce a double cluster structure with strings and compact blobs. A characteristic length is introduced comparing the width of the capillary threshold distribution and gravity effects at the pore scale. We study electrical properties of percolating clusters. Current distributions along percolating clusters are shown to be multifractal and sensitive to the buoyancy.

PACS number(s): 47.55.Mh, 47.55.Kf, 64.60.Ak, 91.45.Vz

I. INTRODUCTION

Invasion percolation [1] has proven to be an accurate description of slow drainage processes in porous media, where a nonwetting fluid deplaces a wetting fluid at such low velocities that capillary forces dominate in comparison to viscous forces. There is good quantitative agreement between experimental results and numerical investigations using the invasion percolation model [2].

With small modifications, the invasion percolation model takes into account effects of buoyancy on the drainage process in addition to the capillary forces [3]. Also in this case there is quantitative agreement between numerical investigations and experiment [5–7].

Another extension of the invasion percolation model has been in the direction of assuming that the disorder it contains has spatial self-affine correlations [8–13].

In the present paper, we study invasion percolation with buoyancy forces containing self-affine correlations. The experimental system we have in mind is a self-affine gouge-filled fracture joint. The gouge makes this system a porous medium, and capillary effects occur during drainage. As the fracture joint is rough, the buoyancy effect comes into play. The roughness is self-affine, and this introduces long-range correlations into the disorder in the invasion percolation model that model the buoyancy forces.

The relevance of such a model may be appreciated through noting that generally oil transport in reservoirs occurs in fractures rather than in the porous reservoir rocks themselves. This is typical in, e.g., chalk or granite formations where the permeability of the rocks is measured in millidarcy.

Self-affinity is defined through scaling properties of the conditional probability function. We assume that the fracture joint is oriented such that it is described through the function $h=h(\vec{r})$, where $\vec{r}=(x,y)$ is a point in the plane defined by the average height of the joint. The conditional probability function is $g(\Delta h,\Delta\vec{r})$, where $\Delta h=h_2-h_1$ and $\Delta\vec{r}=\vec{r}_2-\vec{r}_1$, and gives the probability density that the height of the joint is h_2 at $\vec{r}_2$ given a height h_1 at $\vec{r}_1$. Suppose we scale $\Delta\vec{r}\rightarrow\lambda\Delta\vec{r}$. The joint is self-affine if

$$\lambda^H g(\lambda^H\Delta h,\lambda\Delta\vec{r})=g(\Delta h,\Delta\vec{r}), \tag{1}$$

*Permanent address: Institutt for Fysikk, Norges Teknisk-Naturvitenskapelige Universitet, N-7491 Trondheim, Norway

where H is the Hurst exponent [14]. Assuming that the fracture joint has an area of $L \times L$, we define the width of the joint roughness over this area as $w = \sqrt{\langle h^2 \rangle}$ (remembering that $\langle h \rangle = 0$). Given that the joint is self-affine with a Hurst exponent H, we find that $w \sim L^H$. Thus, when $H < 1$, the joint is asymptotically flat, as $w/L \to 0$ when $L \to \infty$. It has since long been observed that fractures in brittle materials are self-affine [15]. However, many more recent experimental studies of brittle fractures suggest that the Hurst exponent for these systems takes a universal value, i.e., independent of the material that is fracturing, which is close to 0.8 [16–20]. Thus, brittle fracture joints are asymptotically flat.

In earlier studies of invasion percolation with self-affine correlations in the disorder [8–12], the physical system that the authors had in mind was a drainage process in a self-affine fully open fracture. In making a mapping from drainage in this system to a correlated invasion percolation problem, an assumption is made that the inverse of the length scale set by the crack opening dominates with respect to the local curvature of the fluid-fluid interface parallel to the fracture walls. As the fracture opening is self-affine, it may attain large values with the result that the above crucial assumption no longer holds. Thus, the above mapping cannot hold asymptotically large systems, and is therefore only valid in a crossover regime [21].

In the system that we have in mind, and which has been studied experimentally in Ref. [27], the drainage process occurs in a gouge-filled and self-affine fracture joint. A fracture joint consists of two opposite fracture surfaces that have been pulled apart a given distance in the direction orthogonal to the average fracture surface plane. Thus, the aperture is constant all over the fracture.

We study the shape of invasion percolation clusters with trapping. In terms of the equivalent experimental situation, trapping means that to once an island of the original (defending) fluid has been trapped inside the ocean of the invading fluid, its volume does not change. However, it may migrate, and we introduce and study such rules in the invasion percolation algorithm. Other attempts at adding migration rules to the invasion percolation model may be found in [22–26].

Besides the geometrical shapes of the invasion percolation clusters which change profoundly with changing buoyancy, we also study their electrical properties. This provides information of interest that couples to resistivity measurements in an experimental or field situation for that matter. The current distribution in the clusters of the invading liquid also provides tools for studying their geometry. We demonstrate this.

In Sec. II we start by defining the invasion percolation model and its connection with the percolation problem and with slow drainage in porous media. We then describe how buoyancy is added to the invasion percolation model. We emphasize here that when there are gradients in the system due to buoyancy effects, the connection with the percolation problem is more complex, due to physical instabilities (in contrast to numerical) in the invasion percolation algorithm. We end this section by describing how we model migration of clusters of liquid. Section III is devoted to an analysis of the cluster structure obtained with the extended invasion percolation algorithm. The most striking feature is that when the buoyancy effects are strong, a ''blobs-and-strings'' structure

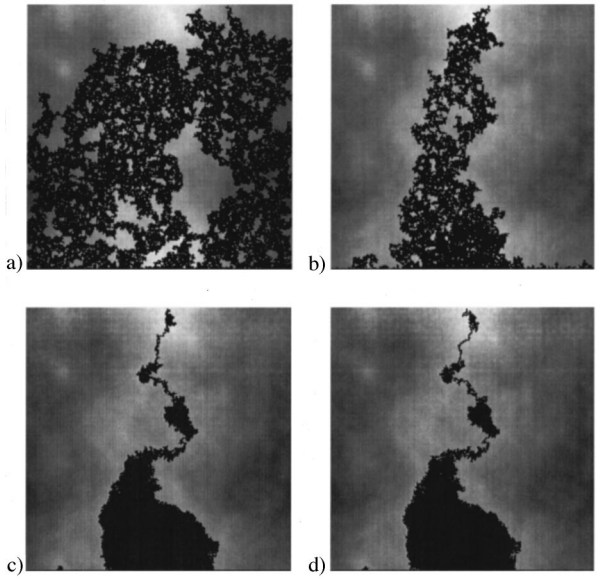

FIG. 1. Four invasion percolation simulations done on the same 256×256 lattice, using injection along the lower edge. We have included trapping effects, but there is no migration. The fluctuation numbers were (a) 10^{-6}, (b) 10^{-2}, (c) 1, and (d) 100. The background shading shows the structure of the self-affine height distribution. Lighter color signifies a higher position. The Hurst exponent of the height distribution is $H = 0.8$, corrersponding to natural brittle fractures.

emerges; see Fig. 1. This is in contrast to the structure of percolation clusters with self-affine disorder. The difference between the two is due to the physical instabilities introduced through the gradients owing to the self-affinity. Figure 1 should be compared to Fig. 2, which shows experimental drainage clusters produced at different gravities, g, $3g$, and $6g$; see Ref. [27]. (These values were obtained by running the injection process in a centrifuge.) Increasing gravity corresponds to the increasing importance of buoyancy. Clearly, a ''blobs-and-strings'' picture emerges as gravity is increased. In Sec. III A, we show how this ''blobs-and-strings'' picture ensues from the hierarchical structure of the self-affine fracture landscape in the limit when buoyancy completely dominates the drainage process. In Sec. III B, we discuss how the competition between buoyancy and capillary effects may be measured through the introduction of a crossover length scale ξ_c. We predict that this length scale obeys certain scaling laws with respect to a dimensionless measure

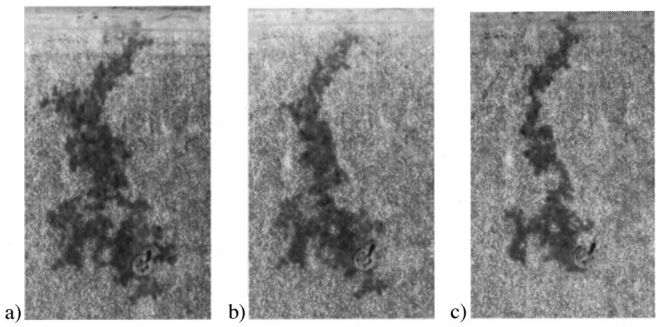

FIG. 2. Experimental drainage clusters at an effective gravity of (a) $1g$, (b) $3g$ and (c) $6g$. (From Ref. [27].)

of the importance of buoyancy and capillary effects, the fluctuation number. We demonstrate the validity of this prediction through numerical experiments. In Sec. IV, we study the electrical transport properties of the drainage clusters. We end by some concluding remarks in Sec. V.

II. MODEL

A. Invasion percolation, percolation, and slow drainage

Before describing our modifications to the original invasion percolation algorithm [1], we explain the latter. We assume a square lattice of size $L \times L$. At each bond ij in the lattice—connecting neighboring nodes i and j—we assign a random number r_{ij} drawn from a uniform distribution on the unit interval. These numbers remain fixed throughout the calculation. In addition to these fixed numbers, each bond has two states: (i) invaded or (ii) not invaded. Let $\varphi_{ij}=0$ signify that bond ij has not been invaded and let $\varphi_{ij}=1$ signify it has been invaded. We initialize the lattice by setting all $\varphi_{ij}=0$. We choose a set of nodes as inlet points in the system. The set consists of all nodes along one of the borders of the lattice. This we call edge injection. We now search among the bonds that are directly attached to the inlet nodes and identify the bond having the smallest random number r_{ij}. We invade this by setting the corresponding $\varphi_{ij}=1$. Assume now that i was one of the inlet nodes. After the invasion of bond ij, node j has become an interface node. In order to proceed with the next injection step, we now search though all bonds connected directly to the inlet nodes *and* the interface nodes, identifying the one with the smallest random number r_{ij} associated with it. This bond is invaded and this algorithm is repeated. We stop the algorithm once any of a given set of outlet nodes have been reached. The outlet nodes are those defining the opposite edge of the lattice.

The physical situation that this algorithm models is slow injection of a nonwetting fluid into a porous medium filled with a wetting fluid. This is drainage. The reason for having the *nonwetting* fluid as the invading fluid is that otherwise film flow may occur, making the use of a binary variable φ_{ij} to describe the state of a bond is impossible. The bond corresponds to a pore in the porous medium. The reason why emphasis is put on *slow* injection is that viscous forces in this limit are negligible in comparison to other relevant forces, which are the capillary and buoyancy forces. For the time being, we assume the porous medium to be two-dimensional and oriented horizontally so that there are no effects of gravity. We are then left with the capillary forces. When the invading fluid is pushed through a pore, the pore shape will determine what pressure is needed, and this value is controlled by the pore neck. The random numbers r_{ij} model the pressures necessary to invade the pores, which are distributed due to the distribution of pore necks.

There is a close relationship between the invasion percolation algorithm and the standard percolation problem [28]. To best demonstrate this relationship, we define the percolation problem in an operational way. Imagine for simplicity a square lattice. Assign to each bond ij a random number r_{ij} drawn from a uniform distribution between zero and one. Introduce a control parameter p. For a given value of p, set all bonds whose random number $r_{ij} \leqslant p$ to ''occupied'' ($\phi_{ij}=1$). The other bonds are unoccupied, $\phi_{ij}=0$. For $p=1$, all bonds will be occupied; for $p=0$, they will all be unoccupied. For intermediate values of p, the occupied bonds will be scattered about in the lattice. We define a cluster of occupied bonds as the set of bonds that are connected through common nodes. Assume now that the lattice is infinite in size. There is then a critical $p=p_c$, the percolation threshold. For $p<p_c$, all clusters of occupied bonds are finite in size. For $p>p_c$, there is one infinite cluster. When $p=p_c$—which is $\frac{1}{2}$ for the square lattice—the system is critical, and the geometry of the clusters has scaling properties described through universal critical exponents.

We now return to invasion percolation. Imagine running the invasion percolation algorithm to a point where N bonds have been invaded. Let us define $r(N)$ as the largest random number r_{ij} that has been picked so far. We now iterate the invasion percolation one more time, and a new random number $r_{ij}^{(N+1)}$ is chosen. Either (i) $r_{ij}^{(N+1)} \geqslant r(N)$ or (ii) $r_{ij}^{(N+1)} < r(N)$. In case (i), we have that $r(N+1)=r_{ij}^{(N+1)}$ and in case (ii) $r(N+1)=r(N)$. Suppose now we make an identical copy of the lattice used for the invasion percolation process, including the same distribution of random numbers r_{ij}. We will use this second copy for percolation. Let us now assume that situation (i) above occurred at the $(N+1)$th iteration of the invasion percolation. Adjusting the percolation control parameter p to the value $p=r(N+1)$ will produce a percolation cluster connected to the inlet nodes that are identical to the invasion percolation cluster at iteration $(N+1)$. (Note that we have not introduced any *trapping rules* so far.) If, on the other hand, situation (ii) occurs, the invasion percolation cluster will be a subset of the percolation cluster connected to the inlet nodes when $p=r(N+1)$. Inverting this argument, we see that for any p there is a corresponding stage in the invasion percolation process where $r_{ij}^{(N+1)}=r(N+1)=p$, and where the cluster in the invasion percolation problem is identical to the cluster in the percolation problem that is connected to the inlet nodes. We also note that the largest value $r(N)$ can attain is the percolation threshold p_c, as the iteration is stopped once any of the outlet nodes are reached. It is, however, important for what follows to note that when the invasion percolation algorithm is stopped at the point when one of the outlet nodes is reached, the system may not be stable. That is to say, the last picked random number r_{ij}, may not be the largest one that has been encountered during the iteration. Thus, there may be a difference between the invasion percolation cluster at this stage and the percolation cluster connected to the inlet nodes with p adjusted to the largest threshold that has been picked.

The physical idea behind the random numbers r_{ij} introduced in the invasion percolation model is that they model the capillary pressure thresholds P_{ij}^t caused by pore necks in the porous medium. If γ is the surface tension, the relation between capillary threshold—measured in units of pressure—and the threshold radius of curvature a_{ij} for invasion of pore ij is

$$P_{ij}^t=\frac{\gamma}{a_{ij}}. \tag{2}$$

In order to perform the slow drainage process, a pressure P must be applied to the injected fluid which is equal to the capillary pressure necessary at a given pore neck in order for

the fluid to invade this pore, $P=P_{ij}^t$. Suppose now that we control the pressure during the injection process. For a given pressure P, we will inject fluid until we reach a situation where all pore necks that are susceptible to injection are so narrow that the pressure necessary to continue is larger than P. The injection process then stops, and only when P is adjusted to a new and sufficiently high value will invasion of further pores occur.

Comparing the invasion percolation model, the percolation model, and the physical drainage problem, we see that the control parameter p in the percolation problem and the pressure P in the drainage problem are related. The relation is the same as between the capillary thresholds P_{ij}^t and the random numbers r_{ij}.

Trapping is built into the invasion percolation algorithm through identifying the clusters of uninvaded bonds surrounded by invaded ones. These are not susceptible to invasion. There is no counterpart to this mechanism in percolation, and with trapping invasion percolation clusters differ from percolation clusters. However, their external perimeters remain identical.

B. Buoyancy effects

In order to introduce buoyancy effects in the invasion percolation model [6], we need to be more precise in defining pressure. There is the threshold capillary pressure necessary at a given interface when situated at some pore neck ij, P_{ij}^t. Let us choose a reference height $h=0$ and consider the corresponding capillary pressure measured at this height. The reference capillary pressure P_{ij} at the height $h=0$ when the pore neck ij is invaded is different from the capillary threshold P_{ij}^t at a height h_{ij}. The subscript ij denotes that this is the capillary pressure necessary to invade pore ij. The invading liquid has a density ρ_i while the defending liquid has a density ρ_d. The gravitational constant is g, and we have that

$$P_{ij}=P_{ij}^t-\Delta\rho g h_{ij}, \tag{3}$$

where $\Delta\rho=\rho_i-\rho_d$. Introducing this effect in the invasion percolation model, the random numbers r_{ij} represent the threshold pressures P_{ij}^t, but the algorithm choosing which bond to invade next should compare the capillary pressures P_{ij} at the reference height $h=0$, not the threshold pressures themselves, P_{ij}^t. Thus, the bond with the smallest P_{ij} that is connected to the inlet nodes or the interface nodes gets invaded next.

The width of the distribution of capillary thresholds is given by

$$w_t=[\langle P_{ij}^{t\,2}\rangle-\langle P_{ij}^t\rangle^2]^{1/2}. \tag{4}$$

It is the width of the capillary pressure distribution which is the important characteristic pressure for the drainage process. Let us assume that the average critical radius of curvature is a. We may then express the pressure involved in the injection process in dimensionless numbers, $\tilde{P}_{ij}=P_{ij}/w_t$, $p_{ij}^t=P_{ij}^t/w_t$, and $\Delta\rho g h_{ij}=F\tilde{h}_{ij}$, where $\tilde{h}_{ij}=h_{ij}/a$ and $F=\Delta\rho g a/w_t$ is the *fluctuation number*. It is this dimensionless number that determines the relative importance of capillary and buoyancy effects in this problem, and Eq. (3) becomes

$$\tilde{P}_{ij}=p_{ij}^t-F\tilde{h}_{ij}. \tag{5}$$

Thus, the invasion percolation algorithm with self-affine buoyancy effects proceeds by assigning random numbers randomly to the bonds in the lattice. The distribution of thresholds p_{ij}^t reflects the pore throat distribution and is generally complex. For our present simulations, we simply chose this distribution to be uniform on the unit interval. If we were to simulate a given cumulative threshold distribution $\Pi(p_t)$, giving the probability to find a threshold value less than p_t, Eq. (5) would become

$$\tilde{P}_{ij}=\Pi^{-1}(r_{ij})-F\tilde{h}_{ij}, \tag{6}$$

where r_{ij} is a random number drawn from a uniform distribution on the unit interval [27]. For the self-affine height distribution, we use the Voss algorithm [4] and assign an h_i to all *nodes i*. Thus, we need to calculate h_{ij}, which is associated to the bond ij from h_i and h_j. A natural choice is an average $h_{ij}=(h_i+h_j)/2$. However, as we will see in Sec. II C, this creates problems when migration is taken into account. We therefore defer further discussion of this point to that section.

Imagine for a moment a flat model oriented at an angle θ *vis à vis* the horizontal. Injection occurs with the lighter fluid at the top edge [5,6]. When $F>0$, the injection process is stable—i.e., does not produce ramified fractal structures (except in a narrow zone whose width is controlled by θ)—and the cluster of the injected fluid may be analyzed in the same way as gradient percolation [29]. However, when the lighter fluid is injected from the bottom, the injection process is unstable [7] and elongated stringy structures ensue. The tilting of the flat model corresponds in terms of the invasion percolation algorithm to setting $h_{ij}=y_j\sin(\alpha)$, where y_j is the distance of node j from the lower edge, in Eq. (3).

It is interesting to note the relation with percolation at this point. When injection is from the top and the process is stable, situation (i), described in Sec. II A, occurs frequently, and when this happens the percolation cluster connected with the inlet nodes that is found by setting p equal to $r(N)$ is equal to the invasion percolation cluster.

However, when injection is from the bottom and the process is unstable, situation (i) will typically *not* occur. That means there will be little resemblance between the invasion percolation cluster and what would have been the corresponding percolation cluster. The stringy structures found in invasion percolation have no correspondent in the percolation problem.

C. Migration effects

Migration occurs when a cluster moves without changing volume. Thus, for each pore invaded by one of the fluids, there is another pore belonging to the perimeter of the same cluster that is invaded by the opposite fluid. The net effect of this is that the cluster moves—and perhaps also changes shape. This is a troublesome effect. Assume that it is the invading, nonwetting fluid that is migrating inside a back-

ground of the defending, wetting fluid. Where it is the migrating cluster that invades bonds, locally one is dealing with a drainage process. However, those bonds that are being invaded by the wetting fluid are experiencing *imbibition*. The trouble with imbibition is the possibility of film flow. Thus, we may encounter a situation where pores are capable of transporting both fluids at the same time. This leads to *nonlocal* effects when attempting to construct a model based on invasion percolation. By nonlocality we mean that a given bond may be occupied by the wetting liquid without sharing any nodes with bonds already occupied with this liquid. Rather than attempting to model these nonlocal effects, we simply ignore them.

When a cluster migrates, for those bonds that are filled or emptied by drainage (a nonwetting fluid replaces a wetting fluid), the mechanism for choosing which bond to invade is identical to the one used in the standard invasion percolation algorithm. However, for those bonds undergoing imbibition (a wetting fluid replaces a nonwetting fluid) during migration, the capillary pressure is close to zero. In the generalized invasion percolation model, we simply set all capillary thresholds related to imbibition to zero. Thus, the critical pressure that is used in determining which bond to update among those susceptible to imbibition, is

$$\tilde{P}_{ij}^{i} = -F\tilde{h}_{ij}. \tag{7}$$

At this point let us use the notation $\tilde{P}_{ij}^{d}$ for the drainage critical pressure defined in Eq. (5).

In order to perform an injection or migration step, we first classify all interfaces in the system. One interface separates the inlet nodes from the outlet nodes. The other interface defines bubbles, or closed-off clusters. For each cluster K, including the one separating the inlet from the outlet, determine among the bonds susceptible to drainage the one with the smallest $\tilde{P}_{ij}^{d}$, which we call $\tilde{P}_{K}^{d}$. Then, determine among the bonds susceptible to imbibition the one with the *largest* $\tilde{P}_{ij}^{i}$, largest since the imbibition process invades a bond in the opposite direction from that of drainage due to the direction of the capillary forces. We call this threshold $\tilde{P}_{K}^{i}$. We then calculate the pressure difference

$$\Delta\tilde{P}_{K} = \tilde{P}_{K}^{d} - \tilde{P}_{K}^{i} \tag{8}$$

of cluster K. When one of the pore necks is drained (i.e., is at the threshold value $\tilde{P}_{K}^{d}$), the pressure difference $\Delta\tilde{P}_{K}$ corresponds to the capillary pressure at the imbibition pore. Then, we search among all clusters K the one that has the smallest $\Delta\tilde{P}_{K}$. If this $\Delta\tilde{P}_{K}$ is positive, all bubbles are stable, and no migration is possible. The bond with the smallest drainage threshold along the interface separating the inlet from the outlet is then invaded. This is an injection step. However, if the minimum $\Delta\tilde{P}_{K}$ is negative, the capillary pressure of one of the pore necks becomes negative and migration occurs. The bond on the interface of the corresponding cluster that is most susceptible to drainage is invaded by the nonwetting fluid, whereas the bond that is most susceptible to imbibition is invaded by the wetting fluid. Migration may occur for any interface, whether it belongs to a bubble or to the interface separating the inlet from the outlet.

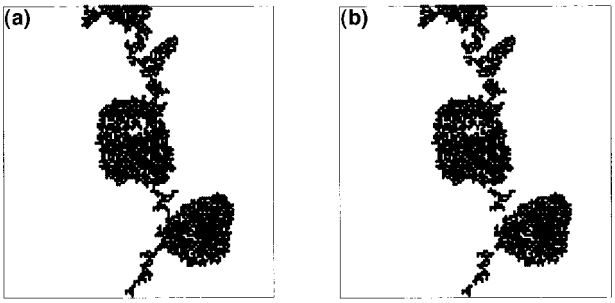

FIG. 3. Effect of migration. In (a), the capillary threshold distribution is uniform on the interval $[s,s+1]$, where $s=10$, while in (b) $s=10^5$. The system size was $L=128$.

The migration algorithm as it has been described so far contains a dangerous instability. The following situation does occur: Once a migration step has been performed, the two bonds that were invaded by the wetting and nonwetting fluids swap roles. That is, the bond that just underwent drainage now becomes the bond that will undergo imbibition next time and vice versa for the other bond. This happens when the bubble is so close to being stable that a *partial* invasion of the two bonds would have sufficed. However, this option is not possible with the present discrete model, and the complete invasion of the two bonds overshoots, so that the bubble is still unstable, but now in the opposite direction. The result is that the algorithm goes into an infinite loop.

This instability is avoided if more care is taken in how $\tilde{h}_{ij}$ is defined. As was mentioned in Sec. II B, the heights are defined at the nodes, and $\tilde{h}_{ij}$ is some function of $\tilde{h}_{i}$ and $\tilde{h}_{j}$. Setting $\tilde{h}_{ij}=(\tilde{h}_{i}+\tilde{h}_{j})/2$ leads to the above instability. However, setting $\tilde{h}_{ij}=\min(\tilde{h}_{i},\tilde{h}_{j})$ in the drainage critical pressure $\tilde{P}_{ij}^{d}$, and $\tilde{h}_{ij}=\max(\tilde{h}_{i},\tilde{h}_{j})$ in the critical imbibition pressure $\tilde{P}_{ij}^{i}$, ensures that both the drainage and the imbibition are maximally stable, and the overshoot is prevented. The instability is cured.

We show in Fig. 3 two drainage clusters. The difference between them is the capillary threshold distributions that were used. In both cases, a uniform distribution was used, but one was shifted compared to the other. That is, the distribution for the left figure was uniform on the interval $[s,s+1]$, where $s=10$, while for the figure on the right, $s=10^5$. In the figure on the left, there is no migration (i.e., continuous cluster), while in the figure on the right, there is migration (i.e., split in discontinuous clusters). We note that the shift s is proportional to the average of the capillary threshold distribution. This is the essential quantity that buoyancy is compared to in defining the Bond number $B=a^2\Delta\rho g/\gamma$. Thus, the Bond number is the proper parameter that controls migration.

III. GEOMETRY OF CLUSTERS

In this section we discuss the geometry of the invasion percolation clusters at various fluctuation numbers, with trapping and with and without migration effects.

A. Infinite fluctuation number

In this limit ($F\to\infty$), gravitational forces dominate completely. We show in Fig. 1(d), a 256×256 lattice with injec-

tion along the lower edge at a fluctuation number $F=100$. As we will demonstrate in Sec. III B, this is sufficiently high for gravity to completely dominate capillary disorder, and the system acts as if F were infinite. In Fig. 1(a), on the other hand, we show the same system, but now at $F=10^{-6}$—which is sufficiently low for any buoyancy effects to be irrelevant. Thus, comparing these two figures, one sees the difference between ''standard'' uncorrelated invasion percolation (a) and correlated invasion percolation with self-affine disorder (d). The striking feature in the infinite-fluctuation number case is the stringy appearance of the cluster—somewhat like beads on a string. This is typical. It is caused by the structure of the self-affine surface.

Self-affine surfaces are hierarchical. They contain valleys within valleys and mountains on mountains. Making a cut through a self-affine surface produces a one-dimensional self-affine profile. The hierarchical structure of the cut may be quantified through the valley size distribution $\mathcal{N}(\Delta,h)$. This is the probability density to find a valley of width Δ a height h above a point on the self-affine profile. That is, draw a horizontal line a height h above the chosen point on the self-affine profile. The horizontal line will cut the self-affine profile at an infinite number of points. The distance between the two cuts that are closest and next closest to where the height h was measured is Δ. In Ref. [30] it was shown that

$$\mathcal{N}(\Delta,h)=\frac{h^{\beta}}{\Delta^{2-H}}G\left(\frac{h}{\Delta^{H}}\right), \tag{9}$$

where $\beta=1/H-1$ and $G(z)$ is a function that tends towards a constant for small arguments and falls off faster than any power law for large arguments, as, e.g., $\exp(-z^2)$ does. Such a power law signifies that the underlying valley structure is hierarchical.

When slow drainage is performed in such a hierarchical landscape for infinite F, the drainage front will constantly change between stable and unstable situations as defined in Sec. II A, where percolation and invasion percolation were compared: The process is stable if the pressure at the inlet must be increased to further advance the invasion front, while it is unstable when the maximum pressure has been reached at some earlier stage of the injection process.

As was described in Sec. II B, when a lighter nonwetting fluid is injected into a heavier, wetting fluid from above in a tilted flat model, the injection is stable and a compact structure ensues, while if the injection is from below, the injection is unstable and the injection structure becomes stringlike.

Thus, in the self-affine landscape, the invasion percolation cluster will consist of a series of ''blobs'' connected by ''strings'' as shown in Fig. 1(d). The blobs occur in the regions where the invasion process is stable. This is where the landscape has a local maximum. As the invasion front reaches a saddle point leading to a region where there is a local maximum, the process will be unstable and it will seek out the most convenient path leading to the local maximum. The result is a stringlike structure. Once the invasion process has reached the maximum, it becomes stable and a compact blob develops around this maximum. This goes on until a new saddle point is reached that leads to another local maximum. The process is from then on unstable until a new maximum has been reached. A new blob then forms around this maximum. This cycle is repeated over and over, resulting in the ''blobs-and-strings'' structure.

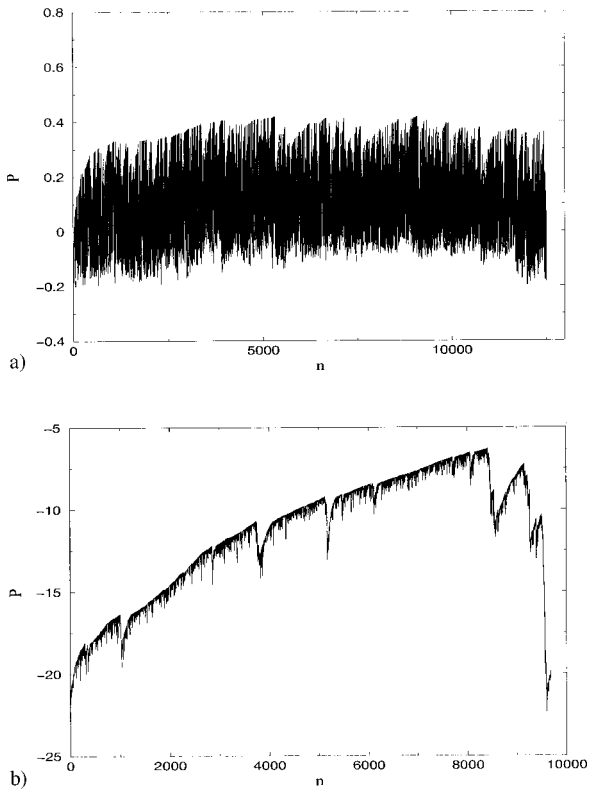

FIG. 4. Injection pressure $\tilde{P}_{ij}$ as a function of the number of invaded bonds for fluctuation number (a) $F=10^{-2}$ and (b) $F=1$.

We record in Fig. 4, the reference capillary pressure $\tilde{P}_{ij}$ as a function of the number of invaded bonds for fluctuation number $F=10^{-2}$ and $F=1$. In Fig. 4(a), where the capillary forces dominate, the pressure develops in a noisy way. The stable regions are those when the $\tilde{P}_{ij}$ at the last invaded bond is larger than all $\tilde{P}_{ij}$ that have occurred before, while the unstable regions are those where this is not true. We see that these regions are intermixed in this case. However, when the fluctuation number $F=1$ [Fig. 4(b)], there is a clear separation between the stable and unstable regions of the signal. It is also clear that the signal is hierarchical in this case. There are local regions where the signal drops within regions that are already unstable. This means that the blobs-and-strings picture is a hierarchical one. As a blob is developing due to a local maximum, the process by which this happens is one that creates blobs and strings at a smaller scale inside the area eventually to be flooded by the developing blob.

In Fig. 5, we show the invaded cluster that gave rise to the pressure curve of Fig. 4(b). The invaded cluster is shown in gray. The black areas consists of those bonds that have a $\tilde{P}_{ij}$ smaller than or equal to the maximum pressure encountered during the injection process, i.e., the percolation clusters. The blob connected to the lower edge of the figure overlaps almost completely with the percolation cluster in the same region. This indicates that the invasion percolation process was stable long enough to completely fill out this region. However, further up in the figure, we see a blobs-and-strings structure entirely inside the percolation cluster. This is caused by the hierarchical structure of the system: This re-

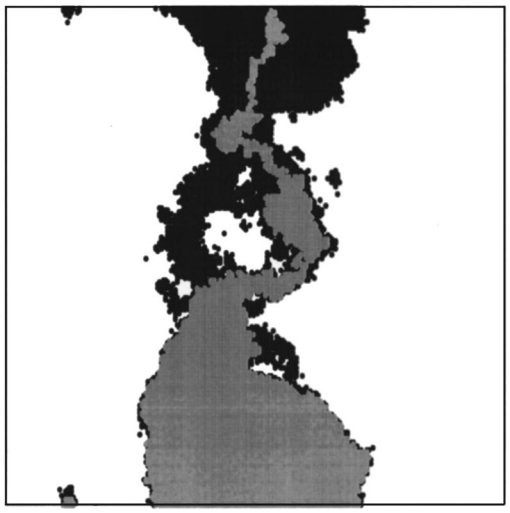

FIG. 5. The invaded cluster (in gray) that gave rise to the pressure curve of Fig. 4(b). The black areas consist of those bonds that have an injection pressure $\tilde{P}_{ij}$ smaller than or equal to the maximum pressure encountered during the injection process, i.e., the percolation clusters.

gion would eventually have been completely filled as the lower one was, but the invasion process reached the upper edge before it was complete. This filling out process proceeds through a blobs-and-strings process at a smaller scale — as described in connection with the pressure curve Fig. 4(b).

B. Finite fluctuation numbers: A crossover length

There is a crossover length between standard invasion percolation and invasion percolation controlled by buoyancy only. The reason for this is as follows. The distribution of injection pressures P_{ij} consists of two independent distributions [see Eq. (3)]: The capillary thresholds p_{ij}^t and the heights h_{ij}. As h_{ij} is self-affine, the width of the distribution is

$$w_h(\xi)/a=[\langle\tilde{h}_{ij}^2\rangle]^{1/2}=(w_a/a)(\xi/a)^H, \tag{10}$$

where ξ is the linear size of the area over which we measure the width and w_a is the width of the distribution at the pore scale: $w_a=w_h(a)$. The width of the distribution of capillary thresholds is

$$w_t=[\langle P_{ij}^{t\,2}\rangle-\langle P_{ij}^t\rangle^2]^{1/2}. \tag{11}$$

The quantity Fw_h/a then reflects the ratio between the width of the hydrostatic pressure distribution and the capillary pressure threshold distribution. When $Fw_h/a\ll 1$, the capillary disorder dominates and the modified invasion percolation algorithm produces standard invasion percolation clusters. In the other limit, when $Fw_h/a\gg 1$, buoyancy dominates and the system behaves as described in Sec. III A. When

$$1=Fw_h(\xi_c)/a, \tag{12}$$

the two disorders balance each other. This equation defines a length scale ξ_c when combined with Eq. (10),

$$\xi_c/a=(w_aF/a)^{-1/H}. \tag{13}$$

On length scales ξ larger than ξ_c, the buoyancy dominates and one sees invasion percolation with self-affine disorder, and with ξ smaller than ξ_c one sees essentially standard invasion percolation.

We see from Eq. (13) that the relevant variable that governs the relative importance of the buoyancy to capillary forces is the fluctuation number.

Returning for a moment to Sec. II C, we may pose a similar question for what determines migration versus injection. The crucial quantity here is the pressure difference $\Delta\tilde{P}_K$ defined in Eq. (8): Is it larger than zero (injection) or smaller than zero (migration)? As the imbibition pressure (7) only depends on the height $\tilde{h}_{ij}$ of the bond susceptible for imbibition while the drainage pressure [see Eq. (5)] depends both on the height and the threshold distribution $\tilde{t}_{ij}$, the question whether migration or injection dominates is answered through comparing the *average* threshold distribution with the *average* height difference across clusters. Thus, it is not the *fluctuation* number F that is relevant here, but rather the bond number B, as has already been pointed out at the end of Sec. II C.

In our simulations, the prefactor w_a in relating horizontal length to vertical height is 0.078, and the Hurst exponent is 0.8. The capillary thresholds are drawn from a flat distribution on the unit interval, and hence $w_t^2=\frac{1}{12}$. We set the lattice constant to unity. Inserted into Eq. (13), we get $\xi_c=1.12/F^{1.25}$. Buoyancy dominates completely when $\xi_c=1$. This gives us a critical fluctuation number of $F_B=1.10$. Capillary disorder dominates, on the other hand, completely in a finite lattice of size L when $\xi_c=L$. This leads to a second critical fluctuation number $F_C=1.10/L^H$. For $L=256$, this gives $F_C=1.3\times10^{-2}$. In Fig. 1 we show a series of invasion percolation simulations done on the same 256×256 lattice, using edge injection. We have included trapping effects, but there is no migration. The fluctuation numbers were 10^{-6}, 10^{-2}, 1, and 100. In Fig. 1(a) we are dealing with standard invasion percolation, as there is no effect from the height distribution. In Fig. 1(d), where the fluctuation number is 100, buoyancy dominates completely. Figure 1(b) is at a fluctuation number very close to $F_C=1.3\times10^{-2}$, while Fig. 1(c) is at a fluctuation number very close to $F_B=1.10$.

In order to measure directly ξ_c, we use the following numerical procedure. Generate a network by distributing heights $\tilde{h}_{ij}$ and thresholds p_{ij}^t. Now, make an exact copy of this network. One of the two identical networks runs the invasion percolation algorithm with the fluctuation number F set to zero, while the other network runs it with the fluctuation number set to the value for which we wish to calculate ξ_c. Record the relative difference between the two clusters that develop, defined as the number of bonds that do not belong to both clusters divided by the number of bonds that has been invaded in either of the two lattices. When this difference has reached a prefixed value, say 10%, stop. We then start from the edge where the invading fluid was injected and compare clusters line for line in the direction perpendicular to this edge. When a difference of 10% has been reached, the distance from the injection edge is ξ_c. In Fig. 6 we show ξ_c as a function of fluctuation number F using 5%,

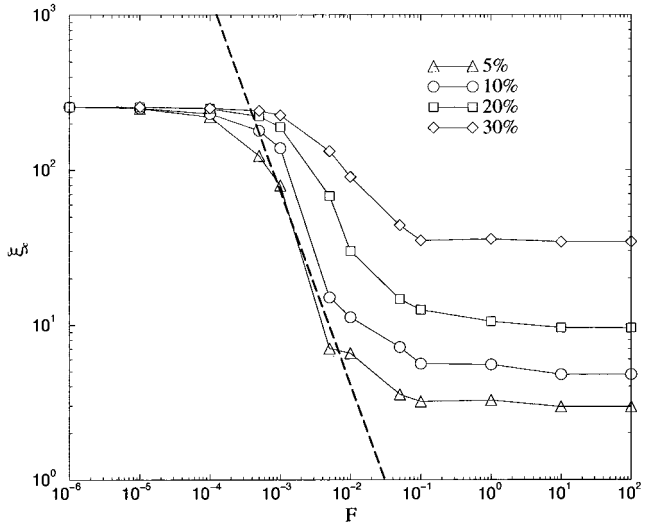

FIG. 6. Evolution of the crossover length ξ_c as a function of fluctuation number F for 5%, 10%, 20%, and 30% difference between invasion clusters at finite and zero fluctuation number. The straight line has a slope of $1/H = 1/0.8 = 1.25$. The system size was 256×256 and each data point is averaged over 100 samples.

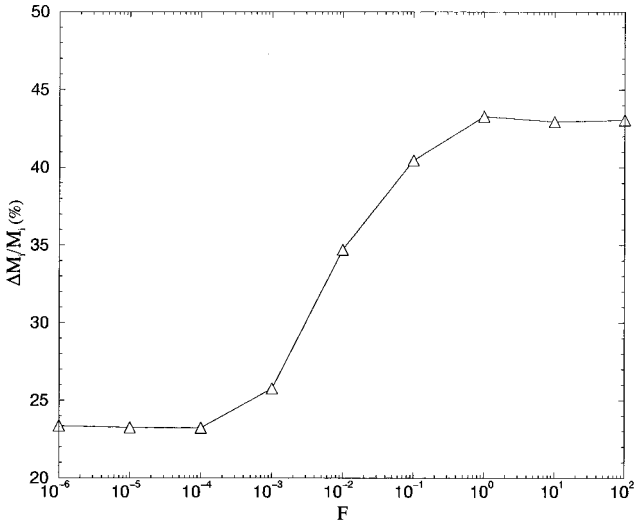

FIG. 8. Evolution of the relative mass fluctuations as a function of the fluctuation number F. Each data point is based on 100 256×256 networks.

10%, 20%, and 30% difference between the two clusters as a basis. The length scale ξ_c becomes less sensitive to the value chosen for the relative difference between the two clusters as this value is decreased: There is hardly any difference between the 5% and the 10% data. We also see that the ξ_c as a function of F follows Eq. (13) for these two data sets. Our theoretical arguments are therefore supported by our simulation results.

Figure 7 shows the invasion clusters for fluctuation numbers $F = 100$ for two different landscapes. There is a huge difference in the size of the two clusters, even though all parameters are the same. We define M_i as the number of invaded bonds at the point when the cluster reaches across the network averaged over different samples. ΔM_i is the sample-to-sample fluctuations (rms) of the same quantity. In Fig. 8, we show the relative mass fluctuations, $\Delta M_i / M_i$, as a function of fluctuation number F. As is evident from this figure, the fluctuations increase dramatically with increasing fluctuation number.

IV. ELECTRICAL TRANSPORT PROPERTIES

We now turn to studying transport properties of the injected clusters. There are several reasons for doing this. One

FIG. 7. Two different self-affine landscapes invaded from the lower edge for a fluctuation number $F = 100$.

is that the invading fluid itself has to be transported through the invaded parts of the porous medium in order to expand further the interface between itself and the invaded fluid. Even though one of the conditions for the invasion percolation algorithm to describe a given physical situation is that viscous forces are negligible compared to the capillary forces, it is not given that the viscous forces may be neglected in studying other phenomena connected to the same invasion process. The viscous forces give rise to the distribution of flow velocities through the different pores. One example where this distribution might be of interest is when the invading fluid contains suspended particles. The time it spends in a given pore will determine how much will sediment in that pore. Thus, knowing the flow velocities will determine the sedimentation patterns in the porous medium.

There might also be quantities other than the invading fluid itself, which is transported through the invading cluster. If, for example, the invading fluid is electrically conducting, electrical current will flow through the invaded pores if a potential difference is set up. The current distribution will, however, be different from the velocity distribution of the invading fluid since the effective electrical conductance distribution of the pores will be different from their permeability distribution.

In this section, we will neglect complications due to permeability and conductance distributions in the transport properties of the invaded cluster. Rather, we will assume that the transport properties of the individual pores are identical. The reason we can do this is that the invasion process we are studying produces fractal clusters. This fractal structure will dominate the transport properties compared to the effect of the disorder that local permeability or conductance variations introduce. As we will see in this section, the current or velocity distribution in clusters with constant pore permeability and conductance is characterizable with power laws. On the other hand, permeability and conductance distributions will induce current distributions that fall off at least as fast as exponentials.

It is the aim of this section to use the current distribution

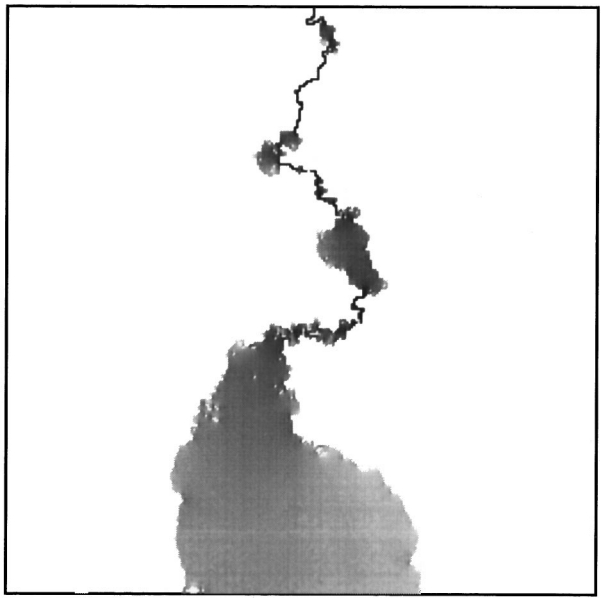

FIG. 9. Current distribution in a percolating invasion cluster with a fluctuation number $F=100$. The lattice size is 256×256. The gray scale reflects the current distribution. Light gray corresponds to very small currents, and darker gray means larger currents until black, which signals that the corresponding bond carries the entire current flowing in the cluster.

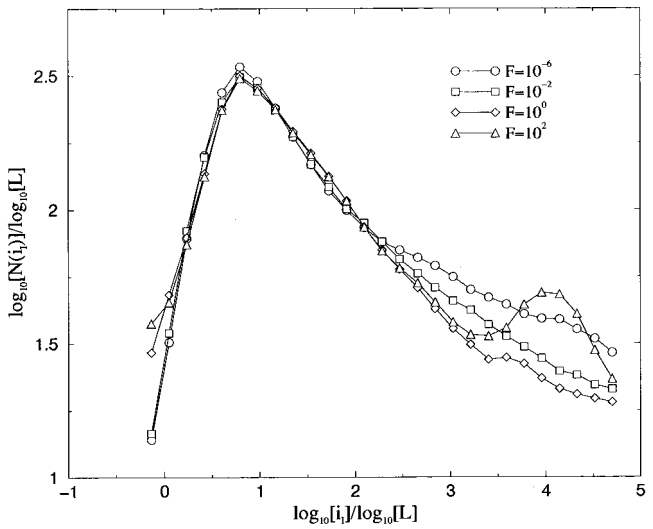

FIG. 10. Histogram of current distribution in percolating invasion clusters with fluctuation numbers $F=10^{-6}$, $F=10^{-2}$, $F=1$, and $F=100$. The lattice sizes were 256×256, and 100 samples were generated for each lattice size and fluctuation number. The total current entering each cluster was set to unity.

in the invaded clusters as a measuring tool to further characterize their geometrical structure. The underlying reason for this suggestion is the rich, multifractal structure of the current distribution in the random resistor network at the percolation threshold that was uncovered in the mid-1980s [31,32]. It is conceivable that the current distribution on the invasion clusters generated at different fluctuation numbers will be as rich in structure as the random resistor network at the percolation threshold. The numerical evidence we present in this section shows that this is indeed so. We also demonstrate how the current distribution depends on the fluctuation number of the invasion process.

The invasion process is run from an injecting border until the invading cluster has reached the opposite border of the network. Both opposite borders are used as electrodes and a potential difference $\Delta V=1$ is set up between them. The current carried by each bond belonging to the invaded cluster is then calculated using a conjugate gradient algorithm [33].

The conductance measured between the two electrodes, G, fluctuates from sample to sample. This results in the total current flowing through the network $I=G\Delta V$ fluctuating likewise from sample to sample. Since we seek to connect the current flow in the bonds with the structure of the clusters to which they belong, it is advisable to move from the *constant voltage ensemble* where the voltage difference across each sample is kept constant to the *constant current ensemble* where the total current flowing in each sample is kept constant. In practice, this is done by calculating G from the current distribution found when $\Delta V=1$, and then normalizing this by dividing each of these currents by G.

We illustrate in Fig. 9 the current distribution for an invading cluster generated with a fluctuation number $F=100$. Bonds carrying large currents have been denoted with dark gray, while bonds carrying smaller currents are drawn with light gray. Note, in particular, the black bonds. These carry a current equal to $I=1$. In the standard terminology of percolation theory, these are the *red* or *cutting* bonds—the first term, because these are the ''hottest'' bonds in the system (from ohmian heating), and the second term because if one of these bonds is cut, the conductivity of the network will drop to zero [28]. As is visible in Fig. 1, the bonds that constitute the invasion cluster falls into two types of structures for high fluctuation numbers: bonds belonging to the blobs and bonds belonging to the strings. The blobs are compact structures, while the strings are not. Clearly, the strings will carry a current equal to or close to the entire current flowing in the cluster, while the bonds belonging to the blobs will carry much lower current as it will be distributed among the bonds in each blob.

In Fig. 10 we show a series of histograms for networks of size 256×256 for different Fluctuation numbers ranging from $F=10^{-6}$ to $F=100$. This figure shows how a ''string peak'' for bond currents i close to one $[\ln(i)=0]$ appears and grows in importance as the fluctuation number F is increased. The other, very broad peak on the left stems from the bonds belonging to blobs. In Fig. 11, we show the number of red bonds as a function of lattice size L. We find that it behaves as a power law,

$$M_{\mathrm{red}}\sim L^{D_{\mathrm{red}}}. \tag{14}$$

Thus, the red bonds form a fractal set with dimension D_{red} equal to 0.08 for $F=10^{-6}$ to 0.67 for $F=100$. (For percolation, $D_{\mathrm{red}}=1/\nu=3/4$ [28].) We see that there is no difference in slope between the $F=10^{-6}$ and $F=10^{-2}$ data sets and the $F=1$ and $F=100$ data sets. This seems to suggest that there are only two classes of behaviors: $D_{\mathrm{red}}=0.08$ for capillary-dominated drainage and $D_{\mathrm{red}}=0.67$ for buoyancy-dominated drainage.

In Fig. 12, we show the distribution of blob sizes, $N(m)$, as a function of the number of bonds belonging to a blob, m. The blobs have been defined as clusters of bonds that are not

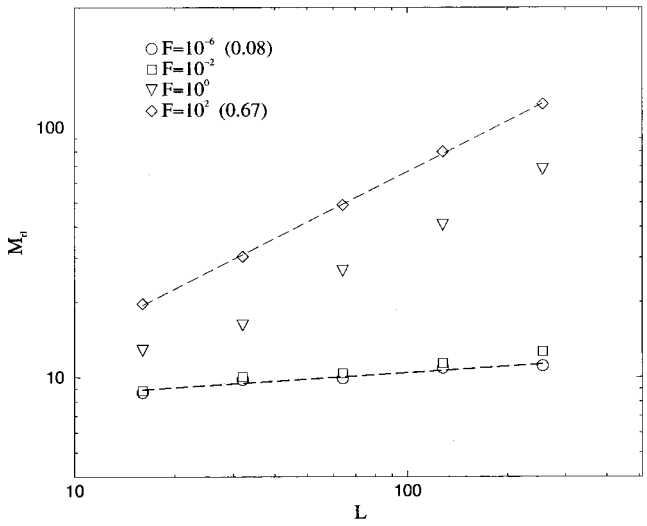

FIG. 11. Total number of red bonds as a function of network size L for different fluctuation numbers F. The data points are averages over 200 samples.

red bonds. In the limit of high fluctuation number F, the blobs are a subset of the islands obtained from a cut of the fracture surface at a given height (see Fig. 5). Distributions of the blob size and of the cut island size have the same behavior. Blobs are shown to be compact with a fractal dimension close to $D_b=2$. Their spatial extension Δ is related to their dimension as $\Delta \sim m^{1/D_b}$. Using Eq. (9), we obtain the following law for the blob distribution:

$$N(m) \sim m^{-1+D_b-H/D_b}. \tag{15}$$

The roughness exponent is $H=0.8$, which leads to the fit

$$N(m) \sim m^{-1.1}, \tag{16}$$

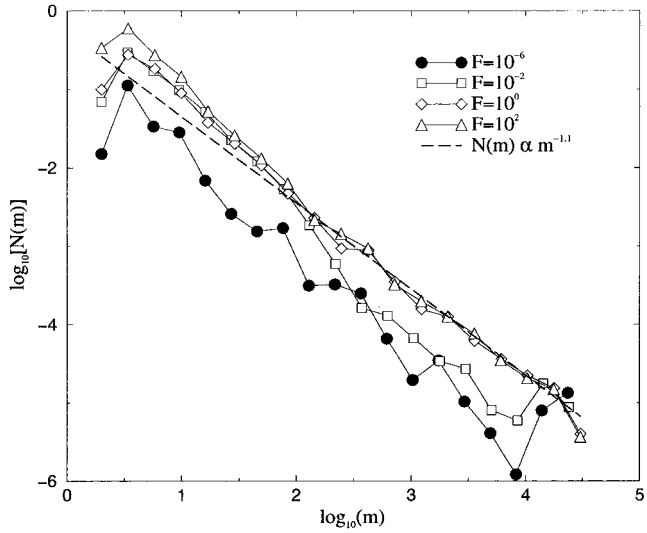

FIG. 12. Distribution of blob sizes. The distribution is computed with logarithmic binning and divided with m to get the distribution corresponding to a linear binning $N(m)$. The system size was 256×256 and 100 samples.

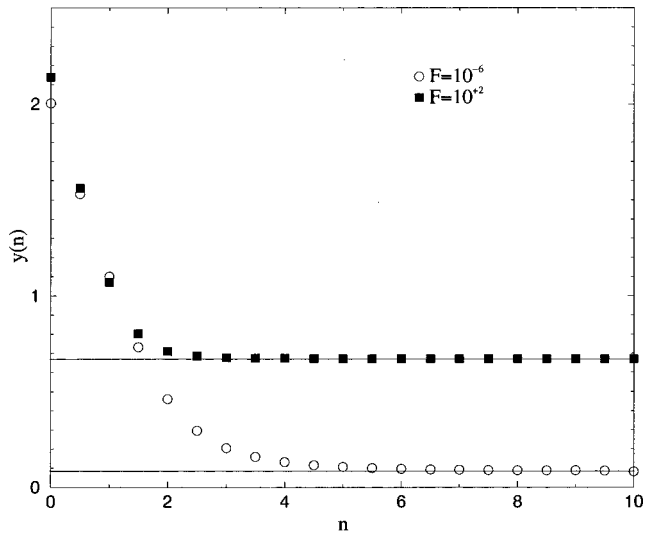

FIG. 13. Evolution of the scaling exponent $y(n)$ as a function of the current moment order n in the constant-current ensemble for two fluctuation numbers: $F=10^{-6}$ and $F=100$. Lattice sizes ranged from $L=32$ to $L=256$. 200 samples were generated for $L=32$, and 100 for the lattice sizes greater than $L=32$.

which is very consistent with the numerical estimate of the blob size distribution for high fluctuation number F (see Fig. 12).

The current distribution in the random resistor network at the percolation threshold was shown to be *multifractal* [31,32]. Multifractality is most easily detected through the scaling properties of the moments of the current distribution. They are defined as

$$\mathcal{M}^{(n)} = \sum i^n N(i,L) \sim L^{y(n)}, \tag{17}$$

where $N(i,L)$ is the current distribution for lattices of size L. The current distribution is multifractal if the scaling exponents $y(n)$ do *not* depend on n as $y(n)=an+b$. Multifractality implies that the proper scale-independent variables to describe the currents and their distribution are $\alpha = \ln(i)/\ln(L)$ and $f(\alpha)=\ln(N(L^{\alpha},L))/\ln(L)$. (We note that the implication does not go the other way; a power-law dependency of N on i would imply the same scale-independent description.)

We show in Fig. 13 the scaling exponents $y(n)$ as a function of n as calculated from the constant-current ensemble for fluctuation numbers $F=10^{-6}$ and $F=100$. In the constant-current ensemble, $y(n)$ must approach the fractal dimension of the red bonds, D_{red} as $n\to\infty$. If the current distribution is not multifractal, this convergence combined with the functional form $y(n)=an+b$ implies that $y(n)=D_{\mathrm{red}}$ independently of n. However, as can be seen from Fig. 13, this is not so. The current distribution is multifractal. It is remarkable that the scaling exponents $y(n)$ for smaller n are so close to each other for the two different fluctuation numbers that we have used. The geometry of the clusters on which the current flows is very different, as can be seen in Fig. 1.

V. CONCLUSIONS

We have studied a generalization of the invasion percolation algorithm to study drainage in a horizontally oriented gouge-filled fracture. The fracture is rough, and this introduces buoyancy effects with self-affine correlations in the model. We also discuss migration effects due to buoyancy. When buoyancy is weak compared to the capillary effects, the invading clusters are those of standard invasion percolation. However, as the importance of buoyancy increases, the structure of the invasion clusters attains a blobs-and-strings structure, see Fig. 1. The blobs-and-strings structure is hierarchical—and therefore fractal—and is caused by the hierarchical structure of the self-affine fracture landscape, where valleys are found within valleys and mountains are superimposed on mountains. We demonstrate that there is a length scale ξ_c that signals the crossover between capillary dominance—and therefore standard invasion-percolation behavior—and dominance of buoyancy, giving rise to the blobs-and-strings structures. The crossover length scale depends on the control parameter F which is the *fluctuation number*. The blob size distribution is analyzed and shown to be consistent with a return probability argument. Lastly, we have studied the transport properties of the invasion cluster. The current distribution of the invasion clusters is multifractal. We also find that the bonds belonging to the strings form a fractal set with fractal dimension either equal to 0.08 when capillary forces dominate or equal to 0.67 when buoyancy dominates.

ACKNOWLEDGMENTS

A.H. thanks the Ecole Normale Supérieure for financial support. We also thank the CNRS and the NFR for support of an exchange program between France and Norway.

[1] D. Wilkinson and J. F. Willemsen, J. Phys. A **16**, 3365 (1983).
[2] R. Lenormand and C. Zarcone, Phys. Rev. Lett. **54**, 2226 (1985).
[3] D. Wilkinson, Phys. Rev. A **30**, 520 (1984).
[4] R. F. Voss, in *Fundamental Algorithms in Computer Graphics*, edited by R. A. Earnshaw (Springer, Berlin, 1985).
[5] J.-P. Hulin, E. Clément, C. Baudet, J. F. Gouyet, and M. Rosso, Phys. Rev. Lett. **61**, 333 (1988).
[6] A. Birovljev, L. Furuberg, J. Feder, T. Jøssang, K. J. Måløy, and A. Aharony, Phys. Rev. Lett. **67**, 584 (1991).
[7] P. Meakin, J. Feder, V. Frette, and T. Jøssang, Phys. Rev. A **46**, 3357 (1992).
[8] P. Meakin, G. Wagner, V. Frette, J. Feder, and T. Jøssang, Fractals **3**, 799 (1995).
[9] C. Du, B. Xu, Y. C. Yortsos, M. Chaouche, N. Rakotomalala, and D. Salin, Phys. Rev. Lett. **74**, 694 (1995).
[10] C. Du, C. Satik, and Y. C. Yortsos, AIChE J. **42**, 2392 (1996).
[11] G. Wagner, P. Meakin, J. Feder, and T. Jøssang, Phys. Rev. E **55**, 1698 (1997).
[12] G. Wagner, P. Meakin, J. Feder, and T. Jøssang (unpublished).
[13] M. Sahimi, Phys. Rep. **306**, 213 (1998).
[14] J. Feder, *Fractals* (Plenum Press, New York, 1988).
[15] B. B. Mandebrot, D. E. Passoja, and A. J. Paullay, Nature (London) **308**, 721 (1984).
[16] E. Bouchaud, G. Lapasset, and J. Planès, Europhys. Lett. **13**, 73 (1990).
[17] K. J. Måløy, A. Hansen, E. L. Hinrichsen, and S. Roux, Phys. Rev. Lett. **66**, 2476 (1992).
[18] J. Schmittbuhl, S. Gentier, and S. Roux, Geophys. Res. Lett. **20**, 639 (1993).
[19] J. Schmittbuhl, F. Schmitt, and C. H. Scholz, J. Geophys. Res. **100**, 5953 (1995).
[20] E. Bouchaud, J. Phys.: Condens. Matter **9**, 4319 (1997).
[21] F. Plouraboué, P. Kurowski, J.-P. Hulin, S. Roux, and J. Schmittbuhl, Phys. Rev. E **51**, 1675 (1995).
[22] G. Wagner, A. Birovljev, P. Meakin, J. Feder, and T. Jøssang, Europhys. Lett. **31**, 139 (1995).
[23] G. Wagner, A. Birovljev, P. Meakin, J. Feder, and T. Jøssang, Physica A **218**, 29 (1995).
[24] A. Birovljev, G. Wagner, P. Meakin, J. Feder, and T. Jøssang, Phys. Rev. E **51**, 5911 (1995).
[25] G. Wagner, A. Birovljev, P. Meakin, J. Feder, and T. Jøssang, Phys. Rev. E **55**, 7015 (1997).
[26] G. Wagner, P. Meakin, J. Feder and T. Jøssang (unpublished).
[27] H. Auradou, K. J. Måløy, J. Schmittbuhl, and A. Hansen (unpublished).
[28] D. Stauffer and A. Aharony, *Introduction to Percolation Theory*, 2nd ed. (Francis and Taylor, London, 1992).
[29] M. Rosso, J. F. Gouyet, and B. Sapoval, Phys. Rev. B **32**, 6053 (1985).
[30] H. Auradou, D. Bideau, A. Hansen, and K. J. Måløy, J. Phys. A **30**, 4915 (1997).
[31] L. de Arcangelis, S. Redner, and A. Coniglio, Phys. Rev. B **31**, 4725 (1985).
[32] R. Rammal, C. Tannous, P. Breton, and A. M. S. Tremblay, Phys. Rev. Lett. **54**, 1718 (1985).
[33] G. G. Batrouni and A. Hansen, J. Stat. Phys. **52**, 747 (1988).